


Article

Basal Ganglia Iron Content Increases with Glioma Severity Using Quantitative Susceptibility Mapping: A Potential Biomarker of Tumor Severity

Thomas P. Reith¹, Melissa A. Prah¹, Eun-Jung Choi², Jongho Lee², Robert Wujek³, Mona Al-Gizawiy¹, Christopher R. Chitambar^{1,4}, Jennifer M. Connelly⁵  and Kathleen M. Schmainda^{1,6,*}

¹ Medical College of Wisconsin, Biophysics, 8701 Watertown Plank Rd., Milwaukee, WI 53226, USA; treith@mcw.edu (T.P.R.); mprah@mcw.edu (M.A.P.); malgizawiy@mcw.edu (M.A.-G.); cchitamb@mcw.edu (C.R.C.)

² Department of Electrical and Computer Engineering, Seoul National University, Seoul 08826, Korea; karaedduk@hanmail.net (E.-J.C.); jonghoyi@snu.ac.kr (J.L.)

³ Medical College of Wisconsin, Biomedical Engineering, Marquette University, 1515 W. Wisconsin Ave., Milwaukee, WI 53233, USA; rwujek@mcw.edu

⁴ Medical College of Wisconsin, Hematology & Oncology, 8701 Watertown Plank Rd., Milwaukee, WI 53226, USA

⁵ Medical College of Wisconsin, Neurology & Neurosurgery, 8701 Watertown Plank Rd., Milwaukee, WI 53226, USA; jconnelly@mcw.edu

⁶ Medical College of Wisconsin, Radiology, 8701 Watertown Plank Rd., Milwaukee, WI 53226, USA

* Correspondence: kathleen@mcw.edu



Citation: Reith, T.P.; Prah, M.A.; Choi, E.-J.; Lee, J.; Wujek, R.; Al-Gizawiy, M.; Chitambar, C.R.; Connelly, J.M.; Schmainda, K.M. Basal Ganglia Iron Content Increases with Glioma Severity Using Quantitative Susceptibility Mapping: A Potential Biomarker of Tumor Severity. *Tomography* **2022**, *8*, 789–797. <https://doi.org/10.3390/tomography8020065>

Academic Editors: Jasper Nijkamp, Lubomir Hadjiyski, Robert J. Nordstrom and Chad Quarles

Received: 10 January 2022

Accepted: 8 March 2022

Published: 15 March 2022

Publisher's Note: MDPI stays neutral with regard to jurisdictional claims in published maps and institutional affiliations.



Copyright: © 2022 by the authors. Licensee MDPI, Basel, Switzerland. This article is an open access article distributed under the terms and conditions of the Creative Commons Attribution (CC BY) license (<https://creativecommons.org/licenses/by/4.0/>).

Abstract: Background and Purpose: Gliomas have been found to alter iron metabolism and transport in ways that result in an expansion of their intracellular iron compartments to support aggressive tumor growth. This study used deep neural network trained quantitative susceptibility mapping to assess basal ganglia iron concentrations in glioma patients. Materials and Methods: Ninety-two patients with brain lesions were initially enrolled in this study and fifty-nine met the inclusion criteria. Susceptibility-weighted images were collected at 3.0 T and used to construct quantitative susceptibility maps via a deep neural network-based method. The regions of interest were manually drawn within basal ganglia structures and the mean voxel intensities were extracted and averaged across multiple slices. One-way ANCOVA tests were conducted to compare the susceptibility values of groups of patients based on tumor grade while controlling for age, sex, and tumor type. Results: The mean basal ganglia susceptibility for patients with grade IV tumors was higher than that for patients with grade II tumors ($p = 0.00153$) and was also higher for patients with grade III tumors compared to patients with grade II tumors ($p = 0.020$), after controlling for age, sex, and tumor type. Patient age influenced susceptibility values ($p = 0.00356$), while sex ($p = 0.69$) and tumor type ($p = 0.11$) did not. Conclusions: The basal ganglia iron content increased with glioma severity. Basal ganglia iron levels may thus be a useful biomarker in glioma prognosis and treatment, especially with regard to iron-based cancer therapies.

Keywords: quantitative susceptibility mapping (QSM); basal ganglia (BG); MRI; brain tumor iron; glioma

1. Introduction

Iron is a double-edged sword in human metabolism: it is necessary for life, yet toxic in excess amounts [1]. As an avid participant in redox reactions, iron is an essential cofactor for enzymes comprising the mitochondrial electron transport chain and is thus needed for normal cellular replication and growth [2]. Yet this same redox reactivity allows iron to accelerate the formation of free radical species, which cause irreparable—and potentially mutagenic—damage to DNA and cellular membranes [3].

Recent research interest has focused on the role of iron in cancer pathogenesis. Epidemiological studies in the 1980s first associated high body iron stores with increased cancer risk [4–6] and subsequent work has revealed two major mechanisms that explain this relationship. First, the oxidative stress and DNA damage that are induced by excess iron contribute to spontaneous oncogenesis [7]. Second, cancer cells demonstrate an increased dependency on iron, which is needed to fuel their rapid growth and proliferation [8]. Accordingly, such cells alter iron import, export, and storage pathways in ways that result in an expansion of an intracellular iron “pool” to support iron-dependent processes that are increased or activated in malignancy [9]. This reprogramming of iron metabolism in the tumor and its microenvironment is thought to be a critical component of tumor cell survival and growth [9,10].

Recent work has revealed these mechanisms at work in the pathophysiology of gliomas: primary brain tumors that arise from the supportive glial cells that surround and protect neurons. Glioblastomas express high amounts of transferrin receptor 1, which is the main mediator of cellular iron uptake [11], and may also express a second transferrin receptor (transferrin receptor 2) that is not present in normal tissue [12]. Moreover, glioblastomas display increased amounts of ferritin, which is the iron storage protein, and may epigenetically upregulate the production of transferrin itself [13]. The pathways of iron uptake and metabolism are thus promising targets for glioblastoma treatment [14]; indeed, disrupting iron homeostasis has been shown to slow tumor proliferation [15].

Historically, brain iron concentrations have been assessed via postmortem histological examination [16,17]. Recent advances in MRI technology, however, now make in vivo detection feasible [18]. The magnetic susceptibility of a material is a physical property that specifies its degree of internal magnetism in response to an applied magnetic field. The majority of biological materials—such as water, fat, and calcium—are weakly diamagnetic and, therefore, have very small negative susceptibility values. Due to its unpaired electron, however, ferric iron is highly paramagnetic; since tissue iron is predominately stored as ferritin complexes, any increases in the bulk magnetic susceptibility of gray matter are thought to reflect iron deposition [19,20]. The most promising technique for detecting variations in tissue iron is quantitative susceptibility mapping (QSM), which reconstructs the magnetic susceptibility of tissue from gradient echo phase sequence data [21]. The validity of QSM in assessing brain iron concentrations has been confirmed by a number of studies [22–24].

We hypothesized that in glioma patients, the increased iron trafficking could extend beyond neoplastic tissue into healthy brain regions. In this study, we used a recently developed deep neural network trained QSM method (QSMnet+ [25,26]) to investigate basal ganglia (BG) iron concentrations in patients with gliomas.

2. Materials and Methods

Subjects: All participants provided written informed consent according to the institutional review board policy in this Health Insurance Portability and Accountability Act compliant study. Consecutive subjects with brain lesions and susceptibility-weighted imaging collected at our Institution between February 2016 and June 2019 were considered for inclusion in this retrospective study. Exclusion criteria were limited to poor image quality and non-glial or unknown tumor types. A neuropathologist provided a diagnosis for all tumors based on 2016 World Health Organization classification criteria [27].

Image Collection and Processing: All MRI exams were performed on a 3.0T MRI system (GE Healthcare, Milwaukee, WI, USA). The data obtained included pre- and post-contrast T1W, T2W, FLAIR, and SWI with acquisition times of 1.7, 2.0, 2.1, 2.1, and 2.1 min, respectively. For the T1W images, a spin echo acquisition was used with: TE = 1.8–1.9 ms, TR = 5.8 ms, flip angle = 10°, and an acquisition matrix of 256 × 192 with a FOV of 220 × 220 mm. A 0.1 mmol/kg intravenous bolus injection of gadobutrol (Gadavist; Bayer Schering Pharma, Berlin, Germany) was administered before the post-contrast images were collected using the same pre-contrast T1W spin echo imaging parameters. For the T2W

images, a gradient echo acquisition was used with: TE = 87.9–88.6 ms, TR = 3987–4746 ms, flip angle = 111° , and an acquisition matrix of 416×416 with a FOV of 220×220 mm². The FLAIR imaging was collected with: TE = 126.3–127.5 ms, TR = 9000 ms, TI = 2250 ms, flip angle = 111° , and an acquisition matrix of 352×224 with a FOV of 220×220 mm². To collect the SWI imaging, a multi-echo gradient echo acquisition was used with: TE = 13.0, 16.7, 20.4, 24.1, 27.8, 31.5, and 35.2 ms, TR = 38.9–39.1 ms, flip angle = 15° , and an acquisition matrix of 288×224 with a FOV of 220×220 mm².

To enable the construction of the QSM maps, SWI information was directly saved as k-space data. Each echo's k-space data were read and then transformed into the image domain. Using coil sensitivities, ASSET unaliasing was performed. The complex unaliased images were separated into real and imaginary parts with gradient warping correction applied separately. Phase images were unwrapped using Laplacian-based unwrapping and the background field was removed using the V-SHARP algorithm [28]. The QSM maps were created using a deep neural network trained method (QSMnet+ [25,26]) and then re-oriented to their starting orientation using the original phase images. The QSM maps were then affinely co-registered to the post-contrast T1W images using FMRIB's Linear Image Registration Tool (FLIRT; <http://fsl.fmrib.ox.ac.uk/fsl/fslwiki/FLIRT> (accessed on 9 January 2022)) [29–31]. Quantitative delta T1 maps [32] were created from the differences in the standardized pre- and post-contrast T1W images using IB Delta Suite™ software (Imaging Biometrics, Elm Grove, WI, USA).

Image and Statistical Analysis: All image analyses were performed using the Horos medical imaging viewer (<http://horosproject.org/> (accessed on 9 January 2022)). ROIs for the caudate, putamen, and globus pallidus were manually drawn onto the individual slices of the QSM images (Figure 1). The mean voxel intensities for all ROIs were averaged across multiple slices to obtain one QSM value per tissue region per patient. The resulting QSM values for the caudate, putamen, and globus pallidus were further averaged to obtain one overall BG (basal ganglia) QSM value for each patient.

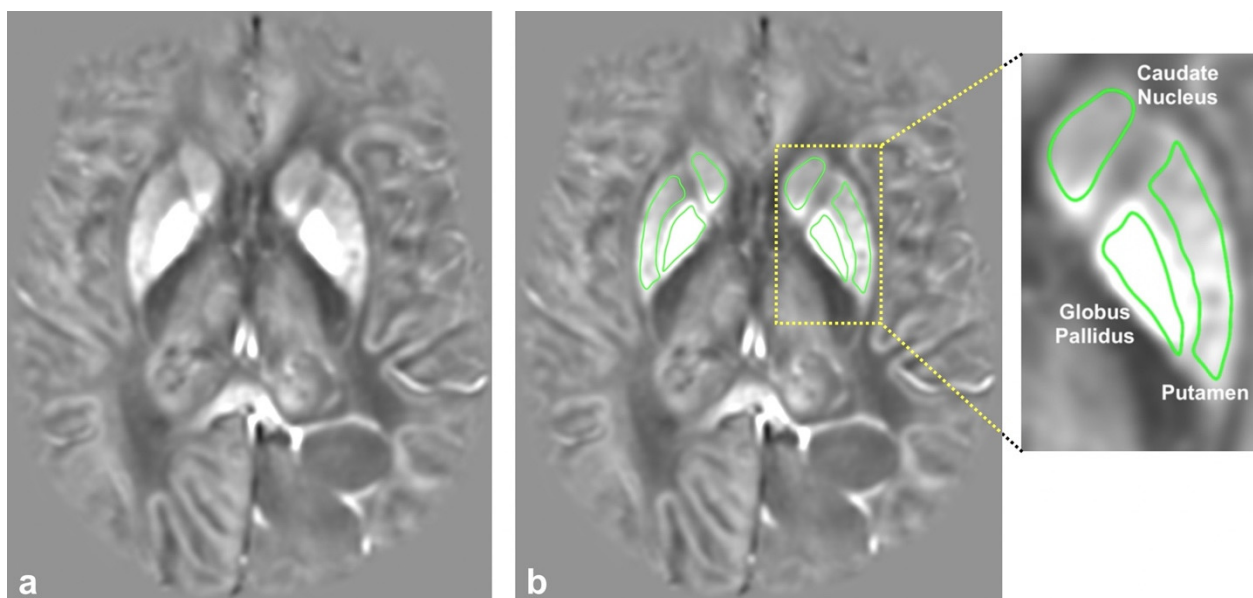


Figure 1. (a) A representative QSM image generated with QSMnet+ and (b) the same QSM image with the regions of interest (ROI) outlines. An enlargement of the left basal ganglia shows the labeled ROIs for the caudate nucleus, putamen, and globus pallidus.

One-way analysis of covariance (ANCOVA) tests were conducted to compare the BG QSM values of the groups of patients based on tumor grade while controlling for age, sex, and tumor type. The normality of the residuals was assessed using the Shapiro–Wilk test and the homogeneity of variances was established using Levene's test.

3. Results

A total of 92 subjects were enrolled in this study. Of these, 12 were excluded due to having non-glial or unknown tumor types, 20 were excluded because the QSM reconstruction process failed, and 1 was excluded because of significant BG distortion resulting from tumor mass effect. After these exclusions, the cohort of subjects that was analyzed consisted of 59 patients (31 males and 28 females) who had been diagnosed with glioma (44 astrocytoma: 7 grade II, 12 grade III, and 25 grade IV; 14 oligodendroglioma: 8 grade II and 6 grade III; 1 gliosarcoma), ranging from 20 to 84 years old (median = 51) for males and 22 to 83 years old (median = 49.5) for females.

Significant differences between the overall mean BG QSM values of the tumor grades were observed after adjusting for age, sex, and tumor type ($F(2,53) = 7.35$, $p = 0.00152$) (Figure 2). Post hoc tests showed that QSM values were significantly higher both in patients with grade IV tumors compared to those with grade II tumors ($p = 0.00153$) and in patients with grade III tumors compared to those with grade II tumors ($p = 0.020$). There were no significant differences between the QSM values of grade III and IV tumors ($p = 0.57$). Age was a significant covariate ($F(1,53) = 9.31$, $p = 0.00356$), while tumor type ($F(1,53) = 2.69$, $p = 0.11$) and sex ($F(1,53) = 0.16$, $p = 0.69$) were not.

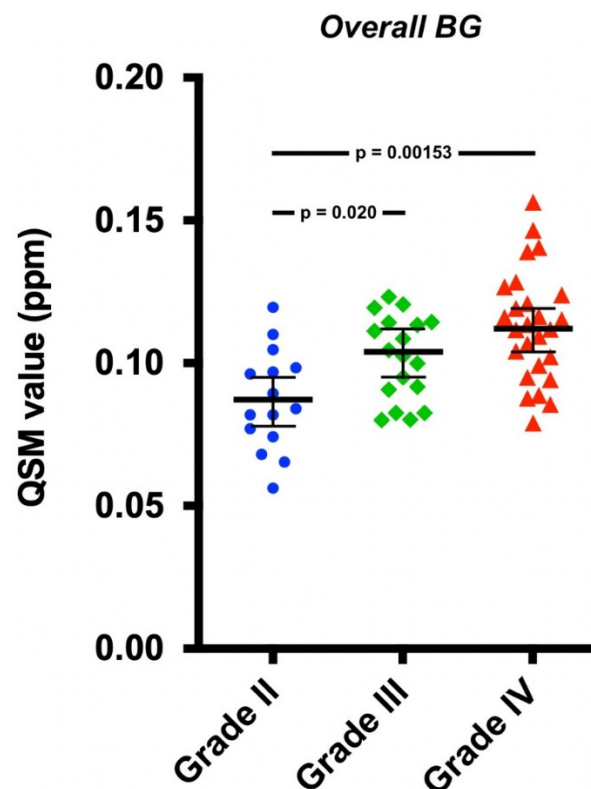


Figure 2. The overall basal ganglia QSM values plotted with covariate adjusted means and standard errors of the means. The means were adjusted for age, sex, and tumor type. The differences were statistically significant between grades II and III and between grades II and IV.

The ANCOVA analysis also revealed significant differences between the QSM values of different tumor grades for the putamen ($F(2,53) = 8.75$, $p < 0.001$) (Figure 3). Post hoc tests showed that QSM values were significantly higher both in patients with grade IV tumors compared to those with grade II tumors ($p < 0.001$) and in patients with grade III tumors compared to those with grade II tumors ($p = 0.034$). There were no significant differences between the putamen QSM values for grade III and IV tumors ($p = 0.14$). No significant differences between the adjusted mean QSM values of different tumor grades were observed for the caudate ($F(2,53) = 2.33$, $p = 0.11$) or the globus pallidus ($F(2,53) = 2.72$, $p = 0.075$).

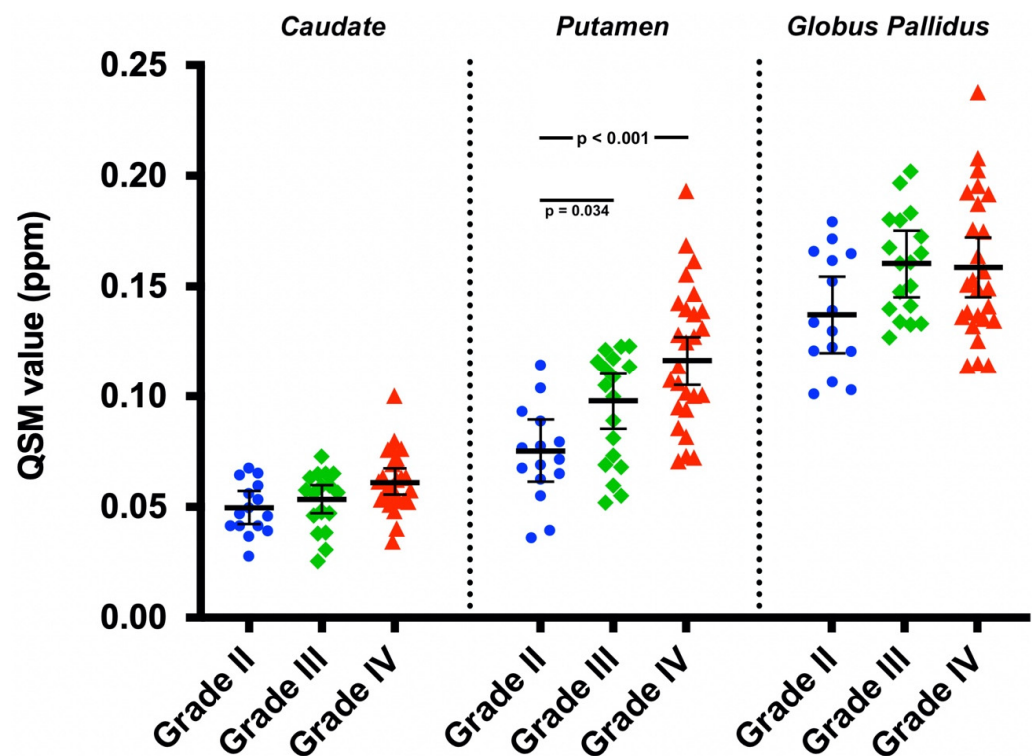


Figure 3. The region-specific basal ganglia QSM values plotted with covariate adjusted means and standard errors of the means. The differences were statistically significant between grades II and III and between grades II and IV for the putamen. The differences for the caudate and globus pallidus were not statistically significant.

After adjusting for age, sex, and tumor grade, no significant differences were found between the overall mean BG QSM values of astrocytoma or oligodendroglioma ($F(1,54) = 3.06$, $p = 0.086$).

Tables 1 and 2 report the covariate adjusted mean QSM values for individual BG regions. Table 3 reports the unadjusted values.

Table 1. The covariate adjusted mean QSM values for patients with tumors of grades II, III, and IV.

	Covariate Adjusted Mean QSM Value (95% CI) (ppm)		
	Grade II	Grade III	Grade IV
Caudate	0.050 (0.042, 0.057)	0.053 (0.047, 0.060)	0.061 (0.055, 0.067)
Putamen	0.075 (0.061, 0.089)	0.098 (0.085, 0.110)	0.116 (0.105, 0.127)
Globus pallidus	0.137 (0.120, 0.154)	0.160 (0.145, 0.175)	0.159 (0.145, 0.172)
Overall BG	0.087 (0.078, 0.096)	0.104 (0.095, 0.112)	0.112 (0.104, 0.119)

Table 2. The covariate adjusted mean QSM values for patients with astrocytoma and oligodendroglioma.

	Covariate Adjusted Mean QSM Value (95% CI) (ppm)
Astrocytoma	
Caudate	0.055 (0.051, 0.059)
Putamen	0.096 (0.089, 0.104)
Globus pallidus	0.151 (0.142, 0.160)
Overall BG	0.101 (0.096, 0.106)
Oligodendroglioma	
Caudate	0.059 (0.051, 0.066)
Putamen	0.112 (0.097, 0.126)
Globus pallidus	0.162 (0.144, 0.180)
Overall BG	0.111 (0.101, 0.121)

Table 3. The unadjusted basal ganglia QSM values for patients with tumors of grades II, III, and IV.

	Mean QSM Value \pm SD (ppm)		
	Grade II	Grade III	Grade IV
All Patients/Tumor			
Types			
Caudate	0.049 \pm 0.012	0.052 \pm 0.013	0.062 \pm 0.014
Putamen	0.073 \pm 0.021	0.094 \pm 0.025	0.119 \pm 0.032
Globus pallidus	0.138 \pm 0.026	0.160 \pm 0.023	0.158 \pm 0.032
Overall BG	0.087 \pm 0.018	0.102 \pm 0.015	0.113 \pm 0.019
Male			
Caudate	0.051 \pm 0.011	0.051 \pm 0.013	0.0611 \pm 0.0080
Putamen	0.073 \pm 0.024	0.094 \pm 0.026	0.116 \pm 0.025
Globus pallidus	0.137 \pm 0.029	0.157 \pm 0.021	0.164 \pm 0.038
Overall BG	0.087 \pm 0.018	0.101 \pm 0.016	0.114 \pm 0.017
Female			
Caudate	0.048 \pm 0.013	0.057 \pm 0.012	0.062 \pm 0.016
Putamen	0.074 \pm 0.020	0.094 \pm 0.029	0.121 \pm 0.036
Globus pallidus	0.140 \pm 0.025	0.169 \pm 0.029	0.155 \pm 0.030
Overall BG	0.087 \pm 0.018	0.1066 \pm 0.0088	0.113 \pm 0.021
Astrocytoma			
Caudate	0.046 \pm 0.013	0.050 \pm 0.015	0.062 \pm 0.014
Putamen	0.067 \pm 0.024	0.084 \pm 0.025	0.119 \pm 0.032
Globus pallidus	0.131 \pm 0.026	0.157 \pm 0.023	0.158 \pm 0.032
Overall BG	0.081 \pm 0.020	0.097 \pm 0.015	0.113 \pm 0.019
Oligodendroglioma			
Caudate	0.052 \pm 0.010	0.0562 \pm 0.0074	–
Putamen	0.079 \pm 0.018	0.1139 \pm 0.0086	–
Globus pallidus	0.144 \pm 0.027	0.166 \pm 0.023	–
Overall BG	0.092 \pm 0.015	0.1120 \pm 0.0094	–

4. Discussion

This study demonstrated the tumor severity-related differences in BG iron content in glioma patients. The results were consistent with a previous preliminary report that demonstrated higher BG iron levels in patients with glioblastoma than in patients with lower grade glioma [33]. The results also agreed with previously reported T2 shortening in the BG and thalamus of 23 patients in with both untreated and recurrent brain tumors compared to healthy controls [34]. The T2 shortening was suggestive of an increased iron concentration that was unaffected by treatment.

Regardless of tumor grade, the globus pallidus consistently had the highest susceptibility, followed by the putamen and caudate nucleus. These differences were consistent with previous studies analyzing BG iron content in both healthy patients and those with a neurodegenerative disease [16,24,35]. For example, the use of QSM in healthy brains was validated by using a comparison to the published estimates of regional brain iron concentrations from postmortem and in vivo data [24]. QSM yielded the same rank ordering of iron concentration by brain structure, with the lowest in white matter and the highest in the globus pallidus, as well as yielding the expected age-related changes. QSM also proved more sensitive than $R2^*$ in assessing changes in brain iron concentration levels in gray matter nuclei for patients with schizophrenia [36], multiple sclerosis [37,38], and Parkinson's disease [39,40].

A natural question raised by our findings is whether the increased BG iron is a direct consequence of tumor development or the BG iron content is suggestive of an iron-rich environment that may promote greater tumor growth or aggression. Paraneoplastic syndromes are a known consequence of many tumors, and glioblastomas in particular may upregulate the production of transferrin [13]. When increased tumor iron trafficking occurs, it is reasonable to assume that this iron may also deposit in nearby structures. In fact, it was hypothesized [34] that an increased iron content in the basal ganglia may represent a

protective process serving to eliminate excessive ferrous ions from the tissue to provide protection from oxidative stress. On the other hand, high levels of both serum [41] and dietary [42] iron are linked to an increased risk of cancer. Therefore, it is possible that some other systemic process leading to increased body iron may contribute to both carcinogenesis and BG deposition. Future research should investigate whether the increased BG iron levels appear before, during or after tumor initiation and growth.

Another question raised regards the mechanism of iron delivery to the BG. Since we observed no contrast agent enhancement in the BG on the quantitative delta T1 maps, the blood–brain barrier was presumably intact and the direct transfer of iron between plasma and tissue was unlikely. However, previously reported elevated levels of ferritin in the cerebrospinal fluid of glioblastoma patients [43] suggest CSF as an alternative means of iron transport to neural tissue.

Potential confounding factors in this study included age and sex. The associations between age and brain iron are well documented, with progressive iron accumulation in the BG accompanying normal aging [35]. Moreover, the incidence of glioblastoma increases exponentially with age [44]. Together, these factors may explain the significant covariance of age in our analysis. Sex, however, was not a significant covariate. Since recent evidence has demonstrated lower levels of BG iron in both pre- and post-menopausal women compared to men [45,46], it is noteworthy that the BG iron accumulation in this study appeared to be independent of the subject's biological sex.

Although the differences between tumor grades were significant for the entire BG, the putamen was the only individual region for which they were significant. The adjusted QSM values for the globus pallidus were also slightly higher for patients with grade III tumors than for patients with grade IV tumors. These observations may be due to the small sample size or additional confounding factors affecting BG iron content that we did not take into account. It is also possible that the putamen alone may better reflect tumor severity than other BG regions. This hypothesis is supported by another recent study in which QSM was used to measure brain iron deposition in patients with type II diabetes mellitus. While decreases in susceptibility were noted for the deep gray matter nuclei of patients compared to healthy controls, the change was only significant for the putamen [47]. While an exact mechanism for this difference is not known, it was concluded that iron levels in the putamen best reflected iron overload injury to the central nervous system.

Overall, there seemed to be a clear trend of increased QSM values associated with more aggressive tumors, suggesting that QSM can be used as an independent measure of tumor aggression and/or may help to further elucidate the role of iron metabolism in brain cancer. Future studies involving larger numbers of patients should address these points.

A final limitation of our study was that no healthy individuals were included due to the lack of available QSM data. Directly comparing the BG QSM values of patients with and without tumors is a logical next step and should be addressed in future work.

5. Conclusions

In this study, we showed that basal ganglia iron content increased with glioma severity. These results demonstrate that in patients with gliomas, increased iron trafficking is not limited to neoplastic tissue but may also occur in healthy brain regions. Basal ganglia iron levels may thus be a useful biomarker in glioma prognosis and treatment, especially with regards to iron-based cancer therapies.

Author Contributions: Conceptualization, C.R.C. and K.M.S.; data curation, T.P.R., R.W., M.A.-G. and K.M.S.; formal analysis, T.P.R., M.A.P., E.-J.C., J.L. and R.W.; funding acquisition, K.M.S.; investigation, J.M.C. and K.M.S.; project administration, K.M.S.; supervision, K.M.S.; writing—original draft, T.P.R. and K.M.S.; writing—review and editing, M.A.P., J.L., R.W., M.A.-G., C.R.C., J.M.C. and K.M.S. All authors have read and agreed to the published version of the manuscript.

Funding: Funding was provided by the Chasing Chad Foundation, Medical College of Wisconsin Cancer Center and NIH/U01 CA176110.

Institutional Review Board Statement: All patient data was obtained in accordance with HIPAA guidelines and after obtaining informed written consent according to guidelines approved by our Institutional Review Board (IRB).

Informed Consent Statement: All subjects provided written, informed consent according to institutional review board policy and the Health Insurance Portability and Accountability Act.

Data Availability Statement: Anonymized data can be made available upon request.

Acknowledgments: We would like to thank Cathy Marszalkowski, Biophysics Research Coordinator, for helping to coordinate the data processing.

Conflicts of Interest: Ownership interest in IQ-AI Ltd. (KMS) and Prism Clinical Imaging Ltd. (KMS) and financial interest in Imaging Biometrics LLC (KMS).

References

1. Youssef, L.A.; Spitalnik, S.L. Iron: A double-edged sword. *Transfusion* **2017**, *57*, 2293–2297. [[CrossRef](#)] [[PubMed](#)]
2. Crichton, R. (Ed.) The Importance of Iron for Biological Systems. In *Iron Metabolism: From Molecular Mechanisms to Clinical Consequences*, 3rd ed.; Wiley Online Books: Hoboken, NJ, USA, 2009; pp. 17–58. [[CrossRef](#)]
3. Dizdaroglu, M.; Jaruga, P. Mechanisms of free radical-induced damage to DNA. *Free Radic. Res.* **2012**, *46*, 382–419. [[CrossRef](#)] [[PubMed](#)]
4. Stevens, R.G.; Beasley, R.P.; Blumberg, B.S. Iron-Binding Proteins and Risk of Cancer in Taiwan. *JNCI J. Natl. Cancer Inst.* **1986**, *76*, 605–610. [[CrossRef](#)] [[PubMed](#)]
5. Stevens, R.G.; Jones, D.Y.; Micozzi, M.S.; Taylor, P.R. Body Iron Stores and the Risk of Cancer. *N. Engl. J. Med.* **1988**, *319*, 1047–1052. [[CrossRef](#)] [[PubMed](#)]
6. Selby, J.V.; Friedman, G.D. Epidemiologic evidence of an association between body iron stores and risk of cancer. *Int. J. Cancer* **1988**, *41*, 677–682. [[CrossRef](#)] [[PubMed](#)]
7. Okada, S. Iron-induced tissue damage and cancer: The role of reactive oxygen species-free radicals. *Pathol. Int.* **2018**, *46*, 311–332. [[CrossRef](#)] [[PubMed](#)]
8. Bystrom, L.M.; Rivella, S. Cancer cells with irons in the fire. *Free Radic. Biol. Med.* **2015**, *79*, 337–342. [[CrossRef](#)] [[PubMed](#)]
9. Torti, S.V.; Torti, F.M. Iron and cancer: More ore to be mined. *Nat. Rev. Cancer* **2013**, *13*, 342–355. [[CrossRef](#)] [[PubMed](#)]
10. Jung, M.; Mertens, C.; Tomat, E.; Brüne, B. Iron as a Central Player and Promising Target in Cancer Progression. *Int. J. Mol. Sci.* **2019**, *20*, 273. [[CrossRef](#)]
11. Voth, B.; Nagasawa, D.T.; Pelargos, P.E.; Chung, L.K.; Ung, N.; Gopen, Q.; Tenn, S.; Kamei, D.T.; Yang, I. Transferrin receptors and glioblastoma multiforme: Current findings and potential for treatment. *J. Clin. Neurosci.* **2015**, *22*, 1071–1076. [[CrossRef](#)]
12. Calzolari, A.; Larocca, L.M.; Deaglio, S.; Finisguerra, V.; Boe, A.; Raggi, C.; Ricci-Vitani, L.; Pierconti, F.; Malavasi, F.; De Maria, R.; et al. Transferrin Receptor 2 Is Frequently and Highly Expressed in Glioblastomas. *Transl. Oncol.* **2010**, *3*, 123–134. [[CrossRef](#)] [[PubMed](#)]
13. Schonberg, D.L.; Miller, T.E.; Wu, Q.; Flavahan, W.A.; Das, N.K.; Hale, J.S.; Hubert, C.G.; Mack, S.C.; Jarrar, A.M.; Karl, R.T.; et al. Preferential Iron Trafficking Characterizes Glioblastoma Stem-like Cells. *Cancer Cell* **2015**, *28*, 441–455. [[CrossRef](#)] [[PubMed](#)]
14. Legendre, C.; Garcion, E. Iron metabolism: A double-edged sword in the resistance of glioblastoma to therapies. *Trends Endocrinol. Metab.* **2015**, *26*, 322–331. [[CrossRef](#)] [[PubMed](#)]
15. Chitambar, C.R.; Al-Gizawi, M.M.; Alhajala, H.S.; Pechman, K.R.; Wereley, J.P.; Wujek, R.; Clark, P.A.; Kuo, J.S.; Antholine, W.E.; Schmainda, K.M. Gallium Maltolate Disrupts Tumor Iron Metabolism and Retards the Growth of Glioblastoma by Inhibiting Mitochondrial Function and Ribonucleotide Reductase. *Mol. Cancer Ther.* **2018**, *17*, 1240–1250. [[CrossRef](#)] [[PubMed](#)]
16. Hallgren, B.; Sourander, P. The effect of age on the non-haemin iron in the human brain. *J. Neurochem.* **1958**, *3*, 41–51. [[CrossRef](#)] [[PubMed](#)]
17. Dexter, D.T.; Wells, F.R.; Agid, F.; Agid, Y.; Lees, A.J.; Jenner, P.; Marsden, C.D. Increased nigral iron content in postmortem parkinsonian brain. *Lancet* **1987**, *330*, 1219–1220. [[CrossRef](#)]
18. Haacke, E.M.; Cheng, N.Y.C.; House, M.J.; Liu, Q.; Neelavalli, J.; Ogg, R.J.; Khan, A.; Ayaz, M.; Kirsch, W.; Obenaus, A. Imaging iron stores in the brain using magnetic resonance imaging. *Magn. Reson. Imaging* **2005**, *23*, 1–25. [[CrossRef](#)]
19. Schenck, J.F.; Dumoulin, C.L.; Redington, R.W.; Kressel, H.Y.; Elliott, R.T.; McDougall, I.L. Human exposure to 4.0-Tesla magnetic fields in a whole-body scanner. *Med. Phys.* **1992**, *19*, 1089–1098. [[CrossRef](#)]
20. Schenck, J.F. The role of magnetic susceptibility in magnetic resonance imaging: MRI magnetic compatibility of the first and second kinds. *Med. Phys.* **1996**, *23*, 815–850. [[CrossRef](#)]
21. Reichenbach, J.R. The future of susceptibility contrast for assessment of anatomy and function. *NeuroImage* **2012**, *62*, 1311–1315. [[CrossRef](#)]
22. Zheng, W.; Nichol, H.; Liu, S.; Cheng, Y.-C.; Haacke, E.M. Measuring iron in the brain using quantitative susceptibility mapping and X-ray fluorescence imaging. *NeuroImage* **2013**, *78*, 68–74. [[CrossRef](#)] [[PubMed](#)]

23. Langkammer, C.; Schweser, F.; Krebs, N.; Deistung, A.; Goessler, W.; Scheurer, E.; Sommer, K.; Reishofer, G.; Yen, K.; Fazekas, F.; et al. Quantitative susceptibility mapping (QSM) as a means to measure brain iron? A post mortem validation study. *NeuroImage* **2012**, *62*, 1593–1599. [[CrossRef](#)] [[PubMed](#)]
24. Bilgic, B.; Pfefferbaum, A.; Rohlfing, T.; Sullivan, E.V.; Adalsteinsson, E. MRI estimates of brain iron concentration in normal aging using quantitative susceptibility mapping. *NeuroImage* **2012**, *59*, 2625–2635. [[CrossRef](#)]
25. Yoon, J.; Gong, E.; Chatnuntawech, I.; Bilgic, B.; Lee, J.; Jung, W.; Ko, J.; Jung, H.; Setsompop, K.; Zaharchuk, G.; et al. Quantitative susceptibility mapping using deep neural network: QSMnet. *NeuroImage* **2018**, *179*, 199–206. [[CrossRef](#)] [[PubMed](#)]
26. Jung, W.; Yoon, J.; Ji, S.; Choi, J.Y.; Kim, J.M.; Nam, Y.; Kim, E.Y.; Lee, J. Exploring linearity of deep neural network trained QSM: QSMnet+. *NeuroImage* **2020**, *211*, 116619. [[CrossRef](#)] [[PubMed](#)]
27. Louis, D.N.; Perry, A.; Reifenberger, G.; von Deimling, A.; Figarella-Branger, D.; Cavenee, W.K.; Ohgaki, H.; Wiestler, O.D.; Kleihues, P.; Ellison, D.W. The 2016 World Health Organization Classification of Tumors of the Central Nervous System: A summary. *Acta Neuropathol.* **2016**, *131*, 803–820. [[CrossRef](#)] [[PubMed](#)]
28. Li, W.; Avram, A.V.; Wu, B.; Xiao, X.; Liu, C. Integrated Laplacian-based phase unwrapping and background phase removal for quantitative susceptibility mapping. *NMR Biomed.* **2014**, *27*, 219–227. [[CrossRef](#)] [[PubMed](#)]
29. Jenkinson, M.; Bannister, P.; Brady, M.; Smith, S. Improved Optimization for the Robust and Accurate Linear Registration and Motion Correction of Brain Images. *NeuroImage* **2002**, *17*, 825–841. [[CrossRef](#)] [[PubMed](#)]
30. Jenkinson, M.; Smith, S. A global optimisation method for robust affine registration of brain images. *Med. Image Anal.* **2001**, *5*, 143–156. [[CrossRef](#)]
31. Greve, D.N.; Fischl, B. Accurate and robust brain image alignment using boundary-based registration. *NeuroImage* **2009**, *48*, 63–72. [[CrossRef](#)]
32. Bedekar, D.; Jensen, T.; Rand, S.; Malkin, M.G.; Connelly, J.; Schmainda, K.M. Delta T1 method: An automatic post-contrast ROI selection technique for brain tumors. In Proceedings of the 18th Annual Meeting and Exhibition of the International Society for Magnetic Resonance in Medicine, Stockholm, Sweden, 1–7 May 2010.
33. Reith, T.; Wujek, R.; Karr, R.; Koch, K.; Al-Gizawiy, M.; Schmainda, K. Basal ganglia iron deposition as a biomarker of brain tumor severity. In Proceedings of the 27th Annual Meeting and Exhibition of the International Society for Magnetic Resonance in Medicine, Montreal, QC, Canada, 11–16 May 2019.
34. Herynek, V.; Wagnerová, D.; Malucelli, A.; Vymazal, J.; Sameš, M.; Hájek, M. Alterations in the basal ganglia in patients with brain tumours may be due to excessive iron deposition. *Oncol. Lett.* **2015**, *9*, 43–46. [[CrossRef](#)]
35. Aquino, D.; Bizzi, A.; Grisoli, M.; Garavaglia, B.; Bruzzone, M.G.; Nardocci, N.; Savoiaro, M.; Chiapparini, L. Age-related Iron Deposition in the Basal Ganglia: Quantitative Analysis in Healthy Subjects. *Radiology* **2009**, *252*, 165–172. [[CrossRef](#)]
36. Xu, M.; Guo, Y.; Cheng, J.; Xue, K.; Yang, M.; Song, X.; Feng, Y.; Cheng, J. Brain iron assessment in patients with First-episode schizophrenia using quantitative susceptibility mapping. *NeuroImage Clin.* **2021**, *31*, 102736. [[CrossRef](#)]
37. Blazejewska, A.I.; Al-Radaideh, A.; Wharton, S.; Lim, S.Y.; Bowtell, R.; Constantinescu, C.; Gowland, P.A. Increase in the iron content of the substantia nigra and red nucleus in multiple sclerosis and clinically isolated syndrome: A 7 Tesla MRI study. *J. Magn. Reson. Imaging* **2015**, *41*, 1065–1070. [[CrossRef](#)]
38. Langkammer, C.; Liu, T.; Khalil, M.; Enzinger, C.; Jehna, M.; Fuchs, S.; Fazekas, F.; Wang, Y.; Ropele, S. Quantitative Susceptibility Mapping in Multiple Sclerosis. *Radiology* **2013**, *267*, 551–559. [[CrossRef](#)]
39. He, N.; Ling, H.; Ding, B.; Huang, J.; Zhang, Y.; Zhang, Z.; Liu, C.; Chen, K.; Yan, F. Region-specific disturbed iron distribution in early idiopathic Parkinson’s disease measured by quantitative susceptibility mapping. *Hum. Brain Mapp.* **2015**, *36*, 4407–4420. [[CrossRef](#)]
40. Langkammer, C.; Pirpamer, L.; Seiler, S.; Deistung, A.; Schweser, F.; Franthal, S.; Homayoon, N.; Katschnig-Winter, P.; Koegl-Wallner, M.; Pendl, T.; et al. Quantitative Susceptibility Mapping in Parkinson’s Disease. *PLoS ONE* **2016**, *11*, e0162460. [[CrossRef](#)]
41. Wen, C.P.; Lee, J.H.; Tai, Y.-P.; Wen, C.; Wu, S.B.; Tsai, M.K.; Hsieh, D.P.; Chiang, H.-C.; Hsiung, C.A.; Hsu, C.Y.; et al. High Serum Iron Is Associated with Increased Cancer Risk. *Cancer Res.* **2014**, *74*, 6589–6597. [[CrossRef](#)]
42. Fonseca-Nunes, A.; Jakszyn, P.; Agudo, A. Iron and Cancer Risk—A Systematic Review and Meta-analysis of the Epidemiological Evidence. *Cancer Epidemiol. Biomark. Prev.* **2014**, *23*, 12–31. [[CrossRef](#)]
43. Sato, Y.; Honda, Y.; Asoh, T.; Oizumi, K.; Ohshima, Y.; Honda, E. Cerebrospinal fluid ferritin in glioblastoma: Evidence for tumor synthesis. *J. Neuro-Oncol.* **1998**, *40*, 47–50. [[CrossRef](#)]
44. Dubrow, R.; Darefsky, A.S. Demographic variation in incidence of adult glioma by subtype, United States, 1992–2007. *BMC Cancer* **2011**, *11*, 325. [[CrossRef](#)] [[PubMed](#)]
45. Persson, N.; Wu, J.; Zhang, Q.; Liu, T.; Shen, J.; Bao, R.; Ni, M.; Liu, T.; Wang, Y.; Spincemaille, P. Age and sex related differences in subcortical brain iron concentrations among healthy adults. *NeuroImage* **2015**, *122*, 385–398. [[CrossRef](#)] [[PubMed](#)]
46. Bartzokis, G.; Tishler, T.A.; Lu, P.H.; Villablanca, P.; Altshuler, L.L.; Carter, M.; Huang, D.; Edwards, N.; Mintz, J. Brain ferritin iron may influence age- and gender-related risks of neurodegeneration. *Neurobiol. Aging* **2007**, *28*, 414–423. [[CrossRef](#)] [[PubMed](#)]
47. Li, J.; Zhang, Q.; Zhang, N.; Guo, L. Increased Brain Iron Deposition in the Putamen in Patients with Type 2 Diabetes Mellitus Detected by Quantitative Susceptibility Mapping. *J. Diabetes Res.* **2020**, *2020*, 7242530. [[CrossRef](#)] [[PubMed](#)]